AD-A105 553 NAVAL RESEARCH LAB WASHINGTON DC F/G 4/1
NONLINEAR EVOLUTION OF PLASMA ENHANCEMENTS IN THE AURORAL IONOS--ETC(U)
OCT 81 M J KESKINEN, S L OSSAKOW
UNCLASSIFIED NRL-MR-4611 NL

END
DATE FILMED
11-81
DTIC

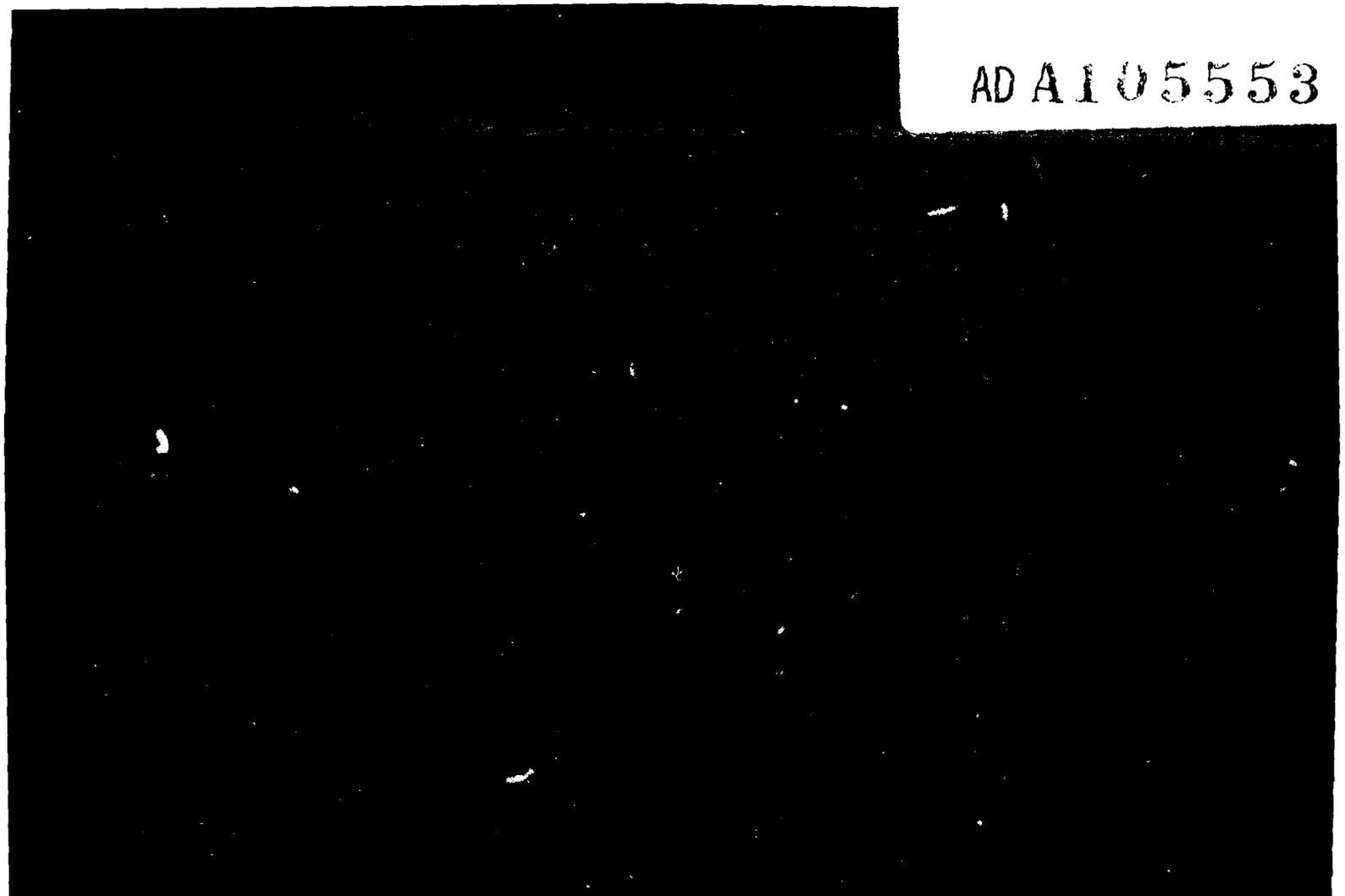
AD A105553

SECURITY CLASSIFICATION OF THIS PAGE (When Data Entered)

REPORT DOCUMENTATION PAGE

READ INSTRUCTIONS BEFORE COMPLETING FORM

1. REPORT NUMBER: NRL Memorandum Report 4611	2. GOVT ACCESSION NO.: AD-A105 553
3. RECIPIENT'S CATALOG NUMBER	
4. TITLE (and Subtitle): NONLINEAR EVOLUTION OF PLASMA ENHANCEMENTS IN THE AURORAL IONOSPHERE I: LONG WAVELENGTH IRREGULARITIES	5. TYPE OF REPORT & PERIOD COVERED: Interim report on a continuing NRL problem.
	6. PERFORMING ORG. REPORT NUMBER
7. AUTHOR(s): M. J. Keskinen and S. L. Ossakow	8. CONTRACT OR GRANT NUMBER(s)
9. PERFORMING ORGANIZATION NAME AND ADDRESS: Naval Research Laboratory, Washington, DC 20375	10. PROGRAM ELEMENT, PROJECT, TASK AREA & WORK UNIT NUMBERS: 61153N; RR033-02-44; 47-0883-0-1; 62704H; 47-0891-0-1
11. CONTROLLING OFFICE NAME AND ADDRESS: Defense Nuclear Agency, Washington, DC 20305 and Office of Naval Research, Arlington, VA 22217	12. REPORT DATE: October 5, 1981
	13. NUMBER OF PAGES: 32
14. MONITORING AGENCY NAME & ADDRESS(if different from Controlling Office)	15. SECURITY CLASS. (of this report): UNCLASSIFIED
	15a. DECLASSIFICATION/DOWNGRADING SCHEDULE

16. DISTRIBUTION STATEMENT (of this Report)

Approved for public release; distribution unlimited.

17. DISTRIBUTION STATEMENT (of the abstract entered in Block 20, if different from Report)

18. SUPPLEMENTARY NOTES

This research was sponsored partially by the Defense Nuclear Agency under Subtask S99QAHC, work unit 00010, work unit title "High Latitude Effects" and partially by the Office of Naval Research.

19. KEY WORDS (Continue on reverse side if necessary and identify by block number)

Plasma enhancements
Auroral ionosphere
Long wavelength irregularities
Numerical simulations
E X B instability
Current convective instability
Power spectrum

20. ABSTRACT (Continue on reverse side if necessary and identify by block number)

The linear stability and nonlinear evolution of plasma enhancements in arbitrary ambient electric fields in the diffuse auroral F region ionosphere have been studied using analytical and numerical simulation techniques. Our results indicate that equatorward convecting plasma slabs initially limited in latitudinal extent are primarily destabilized on their poleward sides by a combination of the effects of convection and field aligned currents. Furthermore we find that the plasma enhancements break up into primary striation-like structures (elongated in the north-south direction for equatorward convection) which can

(Continues)

DD FORM 1 JAN 73 1473 EDITION OF 1 NOV 65 IS OBSOLETE
S/N 0102-014-6601

SECURITY CLASSIFICATION OF THIS PAGE (When Data Entered)

20. ABSTRACT (Continued)

form and cascade from large ($\simeq$ 100 km) to smaller ($\simeq$ 3 km) scale sizes on the order of an hour. The primary and associated smaller scale structures can be oriented either in the north-south or east-west (L-shell alignment) direction depending on the ambient electric field magnitude and direction. For wavenumbers (k_x,k_y) in Fourier space corresponding to the east-west and north-south directions, respectively, the one-dimensional spatial power spectra on the irregularities in the east-west direction $P(k_x) \propto k_x^{-n_x}$ with $n_x \simeq 2\text{-}2.5$ for $2\pi/k_x$ between 100 km and 3 km while in the north-south direction $P(k_y) \propto k_y^{-n_y}$ with $n_y \simeq 2$ for $2\pi/k_y$ between 256 km and 3 km.

CONTENTS

NONLINEAR EVOLUTION OF PLASMA ENHANCEMENTS IN THE AURORAL IONOSPHERE I: LONG WAVELENGTH IRREGULARITIES

1. INTRODUCTION

Recently, large scale equatorward convecting plasma enhancements in the diffuse auroral F-region ionosphere have been identified and studied [Vickrey et al., 1980] using both radar and satellite measurements. Observed in regions of diffuse auroral particle precipitation and associated field aligned currents, these enhancements have overall latitudinal dimensions of a few hundred kilometers, contain relatively steep poleward and equatorward edges, and have been shown to be approximately field-aligned resembling vertical slabs of ionization. Their occurrence, which is maximized in the evening-midnight sector, is apparently not strongly related to magnetic activity nor to E-region processes. The presence of plasma density irregularities associated with these enhancements has been verified using satellite scintillation studies [Fremouw et al., 1977; Rino et al., 1978; Vickrey et al., 1980]. The scintillation data have indicated that the electron density irregularities are structured like L-shell aligned sheets [Fremouw et al., 1977; Rino et al., 1978]. In addition, Rino and Matthews [1979] have shown that the scintillation enhancements resulting from these irregularities cannot be explained in terms of a geometrical enhancement alone. A purely geometrical enhancement occurs when the signal propagation path intercepts an axis transverse to the magnetic field along which axis the irregularities have a high degree of spatial coherence. Moreover, the source region of these scintillation causing irregularities has been demonstrated to be latitude limited [Rino and Owen, 1980] and contained in a vertical slab of F region plasma.

Since these ionization enhancements are observed to convect equatorward, their poleward edges could be unstable to the $\underline{E} \times \underline{B}$ gradient drift instability [Simon, 1963; Linson and Workman, 1970] as observed in artificial ionospheric plasma clouds. Indeed, for observed [Vickrey et al., 1980] poleward

Manuscript submitted July 15, 1981.

density gradient scale lengths of L ≃ 10-50 km and convection velocities of approximately 200 m/sec ($E_o \simeq 10$ mV/m) reasonable growth rates for the $\underline{E} \times \underline{B}$ gradient drift instability can be expected since $\gamma^{-1} \simeq (BL/cE_o) \approx$ 50-250 sec where γ is the $\underline{E} \times \underline{B}$ growth rate, B is the ambient magnetic field and c is the speed of light. Moreover, it has been shown [Ossakow and Chaturvedi, 1979] that by applying the current convective instability [Lehnert, 1958; Kadomtsev and Nedospasov, 1960] the $\underline{E} \times \underline{B}$ stable equatorward side of the plasma enhancements can be driven unstable by the ambient field aligned particle precipitation currents in conjunction with the equatorward density gradients. Other mechanisms that night account for these irregularities are structured low energy particle precipitation and irregular field aligned currents. Keskinen et al. [1980] showed that the nonlinear state of the irregularities in the equatorward edges of these plasma enhancements could be characterized by poleward convecting plasma depletions and equatorward-moving enhancements. In addition, it was demonstrated that these irregularities could be characterized by inverse power laws in the nonlinear regime. However, these studies addressed only the linear and nonlinear evolution of the equatorward side of the plasma enhancements and did not include the $\underline{E} \times \underline{B}$ unstable poleward edge.

In this report we study the stability and nonlinear evolution of "two sided" models of plasma enhancements initially latitudinally confined in order to provide a more realistic picture of the evolution of ionization enhancements in the auroral F region ionosphere. In Section 2 we present a linear stability analysis of the plasma fluid equations which describe the evolution of plasma enhancements in the auroral F region ionosphere. The effects of ambient auroral electric fields of arbitrary magnitude and direction are included. In Section 3 we describe the numerical methods used to solve these equations. The results of these simulations are presented in Section 4 and a discussion of these results is given in Section 5.

2. EQUATIONS OF MOTION AND LINEAR THEORY

For wavelengths greater than the ion mean free path we use fluid equations to describe the ion and electron plasma. The following geometry is used: the y-axis is in the north-south direction, the x-axis points west, and the z-axis is downward along the magnetic field. In this report we ignore the vertical density gradient which is weaker than the horizontal plasma density gradients [Vickrey et al., 1980] in the typical diffuse auroral plasma enhancements. The ion and electron fluids then obey the following equations [Chaturvedi and Ossakow, 1979]:

$$\frac{\partial n}{\partial t} + \nabla\cdot(n\,\underline{v}_e) = 0 \tag{1}$$

$$\frac{\partial n}{\partial t} + \nabla\cdot(n\,\underline{v}_i) = 0 \tag{2}$$

$$\underline{v}_e = \frac{cT_e}{B}\frac{\nabla_\perp n \times \hat{z}}{n} + \frac{c\underline{E}_\perp \times \hat{z}}{B} - \frac{\nu_{ei}c_s^2}{\Omega_e\Omega_i}\frac{\nabla_\perp n}{n} - \frac{eE_z}{m\nu_{ei}}$$

$$-\left(\frac{T_e}{m\nu_{ei}} + \frac{c_s^2}{\nu_{in}}\right)\frac{1}{n}\frac{\partial n}{\partial z}\,\hat{z} + v_o\hat{z} \tag{3}$$

$$\underline{v}_i = \frac{c\underline{E}_\perp \times \hat{z}}{B} + \frac{\nu_{in}}{\Omega_i}\frac{c\underline{E}_\perp}{B} - \frac{cT_i}{eB}\frac{\nabla_\perp n \times \hat{z}}{n} - \frac{\nu_{in}cT_i}{\Omega_i\, eB}\frac{\nabla_\perp n}{n}$$

$$-\frac{\nu_{ei}}{\Omega_e}\frac{c_s^2}{\Omega_i}\frac{\nabla_\perp n}{n} - \frac{c_s^2}{\nu_{in}}\frac{1}{n}\frac{\partial n}{\partial z}\,\hat{z} + V_o\hat{z} \tag{4}$$

$$\nabla\cdot\underline{J} = 0 \tag{5}$$

Here n_α (α = i or e) is the species density and $\underline{E}$ is the total electric field. Since we will be interested in low frequencies and long wavelengths, we have ignored inertial terms in the electron and ion momentum equations

(3) and (4). Equation (5) results from the assumption of quasineutral fluctuations $n_e \simeq n_i \equiv n$. In addition, v_o and V_o refer to the electron and ion velocities along the magnetic field giving rise to the diffuse auroral current. The symbol ν_{in} denotes the ion-neutral collision frequency, ν_{ei} the electron-collision frequency, c the speed of light, $T_e \simeq T_i \equiv T$ the species temperature, c_s the ion acoustic speed and $\Omega_i (\Omega_e)$ the ion (electron) gyrofrequency. We have neglected ν_{en} compared with ν_{ei} and taken $\nu_\alpha/\Omega_\alpha \ll 1$ for $\alpha = i,e$ (F region approximation).

Any two of equations (1), (2), and (5) provide a complete description of the problem. We will use the ion continuity equation (1) and (5). After separating the total electric field into an ambient and fluctuating part $\underline{E}_\perp = \underline{E}_o - \nabla_\perp \delta\varphi$ and transforming to a frame drifting with velocity $\underline{V}_o = -(c/B)\,[\hat{\underline{z}} \times \underline{E}_o - (\nu_{in}/\Omega_i)\underline{E}_o]$ we can write

$$\frac{\partial n}{\partial t} + \frac{c}{B}\left[\hat{\underline{z}} \times \nabla_\perp \delta\varphi \cdot \nabla_\perp n - (\nu_{in}/\Omega_i)\nabla_\perp \delta\varphi \cdot \nabla_\perp n\right] =$$

$$\left(\frac{\nu_{in}}{\Omega_i}\,\frac{cT_i}{eB} + \frac{\nu_{ei}}{\Omega_e}\,\frac{c_s^2}{\Omega_i}\right)\nabla_\perp^2 n + \frac{c_s^2}{\nu_{in}}\,\frac{\partial^2 n}{\partial z^2} \tag{6}$$

$$\nabla_\perp \cdot (n\nabla_\perp \delta\varphi) + \frac{\Omega_i\,\Omega_e}{\nu_{in}\nu_{ei}}\,\frac{\partial}{\partial z}\left(n\,\frac{\partial \delta\varphi}{\partial z}\right) = \left(\underline{E}_o - \frac{\Omega_i}{\nu_i}\,\frac{B}{c}\,\underline{V}_d\right)\cdot \nabla n$$

$$- \frac{T}{e}\left(\nabla_\perp^2 n - \frac{\Omega_i\,\Omega_e}{\nu_{in}\nu_{ei}}\,\frac{\partial^2 n}{\partial z^2}\right) \tag{7}$$

where $\underline{V}_d = \hat{\underline{z}}(v_o - V_o)$. Linearizing (6) and (7) by separating $n = n_o(y) + \delta n$ with $\delta n,\ \delta\varphi \propto \exp[i(k_x x + k_y y + k_z z - \omega t)]$, $\omega = \omega_r + i\gamma$, $kL \gg 1$, $L^{-1} \equiv (1/n_o)(\partial n_o/\partial y)$ we find a growth rate ($k_\parallel \equiv k_z$)

$$\gamma = \frac{-\cos\alpha \frac{\nu_{ei}}{\Omega_e}\frac{1}{L}\left[\frac{\nu_{in}}{\Omega_i}\frac{cE_o}{B}\cos(\alpha-\beta) - \frac{k_z}{k_\perp}V_d\right]}{\frac{k_z^2}{k_\perp^2} + \frac{\nu_{in}}{\Omega_i}\frac{\nu_{ei}}{\Omega_e}} - D_\perp k_\perp^2 - D_\parallel k_z^2 \quad (8)$$

where we have assumed $\underline{k}_\perp = k_x\hat{\underline{x}} + k_y\hat{\underline{y}} = \hat{\underline{x}}\, k_\perp \cos\alpha + \hat{\underline{y}}\, k_\perp \sin\alpha$ and $\underline{E}_o = E_o \cos\beta\hat{\underline{x}} + E_o\sin\beta\, \hat{\underline{y}}$ with $k_\perp^2 = k_x^2 + k_y^2$, $k_\perp^2 \gg k_z^2$, $D_\perp = (\nu_{ei}/\Omega_e\Omega_i)c_s^2$ and $D_\parallel = (c_s^2/\nu_{in})\left\{1 + \left[(\nu_{in}/\Omega_i)^2/\left((\nu_{ei}\nu_{in}/\Omega_e\Omega_i) + (k_z^2/k_\perp^2)\right)\right]\right\}$. The growth rate γ in eq. (8) is maximized for k-vectors propagating at angles α satisfying

$$\sin(2\alpha-\beta) = \zeta \sin\alpha \quad (9)$$

where $\zeta = (k_z/k_\perp)(\Omega_i/\nu_{in})(BV_d/cE_o)$ and we have taken $k_z/k_\perp$ to be fixed. For typical parameters, $k_z/k_\perp \simeq 10^{-4}$, $\nu_{in}/\Omega_i \simeq 10^{-4}$, $v_d \simeq 60$ m/sec ($j_\parallel = 1\ \mu A/m^2$ at a density of $n_o = 10^5 cm^{-3}$) and $E_o = 10$ mV/m ($cE_o/B \simeq 200$ m/sec) we find $\zeta \simeq 0.3$. To lowest order for fixed β we find from (9) the result that $\alpha \simeq \beta/2 + \frac{\zeta}{2}\sin(\beta/2)$. In other words, for $\beta \neq 0$, the linear growth rate maximizes away from the direction perpendicular to the initial density gradient by the angle $\alpha \simeq \beta/2 + \frac{\zeta}{2}\sin(\beta/2)$. As a result the maximum growth rate from (8) can be written to lowest order

$$\gamma = \frac{-\cos(\beta/2)\frac{\nu_{ei}}{\Omega_e}\frac{1}{L}\left[\frac{\nu_{in}}{\Omega_i}\frac{cE_o}{B}\cos(\beta/2) - \frac{k_z}{k_\perp}V_d\right]}{\frac{k_z^2}{k_\perp^2} + \frac{\nu_{in}}{\Omega_i}\frac{\nu_{ei}}{\Omega_e}} - D_\perp k_\perp^2 - D_\parallel k_z^2 \quad (10)$$

For ambient electric fields perpendicular to the initial density gradient ($\beta = 0$), eq. (8) implies that the maximum growth rate occurs for $\alpha = 0$, i.e., $\underline{k}$ along $E_o\hat{\underline{x}}$. This can be written

$$\gamma = \frac{-\frac{\nu_{ei}}{\Omega_e}\frac{1}{L}\left(\frac{\nu_{in}}{\Omega_i}\frac{cE_o}{B} - \theta V_d\right)}{\theta^2 + \frac{\nu_{in}}{\Omega_i}\frac{\nu_{ei}}{\Omega_e}} - D_\perp k_x^2 - D_\parallel k_z^2 \qquad (11)$$

where $\theta \equiv k_z/k_x$. Note that by comparing eq. (10) and (11) the linear growth rate, for arbitrary $\underline{k}$, is reduced when $\underline{E}_o$ is not exactly perpendicular to ∇n_o, i.e., $\beta \neq 0$ because of the $\cos^2(\beta/2)$ factor in (10). In regions of the plasma enhancements where $\partial n_o/\partial y < 0$ and for wavelengths whose perpendicular and parallel diffusive damping are negligible we find the condition for unstable growth $[(\nu_{in}/\Omega_i)(cE_{ox}/B) + \theta|V_d|] > 0$ where we have taken, for example, the currents to be downward, i.e., $V_d < 0$. For westward electric fields $E_{ox} > (B/c)(\Omega_i/\nu_{in})|\theta|\ |V_d|$, the effects of the field-aligned currents will be to reduce ($\theta < 0$) or enhance ($\theta > 0$) the $\underline{E} \times \underline{B}$ instability growth rate. However, when $\partial n_o/\partial y > 0$ the condition for unstable growth becomes $[(\nu_{in}/\Omega_i)(cE_{ox}/B) + \theta|V_d|] < 0$ and could be satisfied for large enough currents with $|V_d| > (\nu_{in}/\Omega_i)(cE_{ox}/B|\theta|)$ if $\theta < 0$. The expression for the growth rate γ in equation (11) can be maximized as a function of $\theta = k_\parallel/k_x$, a measure of field-alignment, using $\partial\gamma/\partial\theta|_{\theta=\theta_m} = 0$ giving

$$\theta_m = \frac{\nu_{in}}{\Omega_i}\frac{cE_{ox}}{B\,V_d} \pm \left[\left(\frac{cE_{ox}}{B\,V_d}\right)^2\left(\frac{\nu_{in}}{\Omega_i}\right)^2 + \left(\frac{\nu_{ei}\nu_{in}}{\Omega_e\,\Omega_i}\right)\right]^{1/2} \qquad (12)$$

Using typical diffuse auroral F region parameters $\nu_{in}/\Omega_i \simeq 10^{-4}$, $\nu_{ei}/\Omega_e \simeq 10^{-4}$ $E_{ox} \simeq 10$ mV/m, $j_\parallel = n_o e V_d \simeq 1\ \mu A/m^2$, $B = 0.5G$, $n_o \simeq 10^5 cm^{-3}$ this gives $|\theta_m| \simeq 10^{-4}$, i.e., approximate field alignment. Inserting these parameters into eq. (11) with $L \simeq 20$ km, $D_\perp \simeq 0.2\ m^2/sec$ and $D_\parallel \simeq 10^8 m^2/sec$ we find that the fastest growing linear modes have growth times $\gamma_{max}^{-1} \simeq 10^2$ sec.

3. NUMERICAL SIMULATIONS

Equations (6) and (7) can be written in dimensionless form by introducing the following scaled quantities $\tilde{n} = n_o/N_o$, $\tilde{\delta\varphi} = \delta\varphi/BL$, $\tilde{x} = x/L$, $\tilde{y} = y/L$, $\tilde{z} = z/L$, $\tilde{t} = ct/L$ as follows (where we have dropped the tilde for clarity)

$$\frac{\partial n}{\partial t} + \frac{\partial \delta\varphi}{\partial x}\frac{\partial n}{\partial y} - \frac{\partial \delta\varphi}{\partial y}\frac{\partial n}{\partial x} - c_1\left(\frac{\partial \delta\varphi}{\partial x}\frac{\partial n}{\partial x} + \frac{\partial \delta\varphi}{\partial y}\frac{\partial n}{\partial y}\right) = c_2\left(\frac{\partial^2 n}{\partial x^2} + \frac{\partial^2 n}{\partial y^2}\right) + c_3\frac{\partial^2 n}{\partial z^2} \qquad (13)$$

$$\frac{\partial^2 \delta\varphi}{\partial x^2} + \frac{\partial^2 \delta\varphi}{\partial y^2} + \frac{1}{n}\left(\frac{\partial n}{\partial y}\frac{\partial \delta\varphi}{\partial y} + \frac{\partial n}{\partial x}\frac{\partial \delta\varphi}{\partial x}\right) + c_4\left(\frac{\partial^2 \delta\varphi}{\partial z^2} + \frac{1}{n}\frac{\partial n}{\partial z}\frac{\partial \delta\varphi}{\partial z}\right)$$

$$= c_5\frac{\partial n}{\partial x} + c_6\frac{\partial n}{\partial y} - c_7\frac{\partial n}{\partial z} - c_8\frac{1}{n}\left(\frac{\partial^2 n}{\partial x^2} + \frac{\partial^2 n}{\partial y^2}\right) + c_9\frac{1}{n}\frac{\partial^2 n}{\partial z^2} \qquad (14)$$

with c_i, $i = 1, \ldots, 9$ dimensionless constants given by $c_1 = \nu_{in}/\Omega_i$, $c_2 = (\nu_{in}/\Omega_i)(T_i/eBL) + (\nu_{ei}/\Omega_e)(c_s^2/\Omega_i cL)$, $c_3 = c_s^2/\nu_{in}cL$, $c_4 = \Omega_e\Omega_i/\nu_e\nu_i$, $c_5 = E_{ox}/B$, $c_6 = E_{oy}/B$, $c_7 = (\Omega_i/\nu_i)(V_d/c)$, $c_8 = T/eBL$, $c_9 = (\Omega_e\Omega_i/\nu_e\nu_i)\,c_8$.

In the following numerical simulations we take advantage of the fact that the fastest growing, most dangerous modes from linear theory are almost field-aligned, i.e., $k_\parallel/k_\perp \ll 1$ where $k_\parallel(k_\perp)$ is the component of $\underline{k}$ parallel (perpendicular) to the magnetic field. These waves are of most interest to us and, as a result, we solve equations (13) and (14) in a plane containing these modes which is nearly perpendicular to the magnetic field while fixing the value of $k_\parallel/k_x \ll 1$. A similar approach has been adopted in numerical studies of drift-wave [Lee and Okuda, 1976] and trapped-particle [Matsuda and Okuda, 1976] instabilities in laboratory plasmas. The system of equations (13) and (14) was first transformed to the $x'y'z'$ coordinate system (as shown in Fig. 1) by a simple rotation about the y-axis by the angle $\theta = k_\parallel/k_x \ll 1$ using

$$\frac{\partial}{\partial x} = \cos\theta \frac{\partial}{\partial x'} - \sin\theta \frac{\partial}{\partial z'}$$

$$\frac{\partial}{\partial z} = \sin\theta \frac{\partial}{\partial x'} + \cos\theta \frac{\partial}{\partial z'}$$

$$\frac{\partial}{\partial y} = \frac{\partial}{\partial y'}$$

where θ is the angle for maximum linear growth rate defined by eq. (12) for a definite set of a parameters ν_{in}/Ω_i, cE_{ox}/BV_d, ν_{ei}/Ω_e. Since $\theta \ll 1$ this transformation can be written $\partial/\partial x \simeq \partial/\partial x'$, $\partial/\partial z \simeq \theta\, \partial/\partial x'$, $\partial/\partial y = \partial/\partial y'$ with $\partial/\partial z \simeq 0$. As a consequence the three dimensional problem is reduced to two-dimensions. By solving equations (13) and (14) in the $x'y'z'$ coordinate system a small but finite $k_\parallel$ is effectively introduced into the model.

Equations (13) and (14) were then solved numerically on a mesh consisting of 258 grid points in the north-south direction (y-direction) and 102 grid points in the east-west direction (x-direction) with constant grid spacing of 1 km. As a result, the simulation plane, which is taken to be essentially horizontal at an altitude of 350 km in the diffuse auroral F region, has a north-south and east-west extent of 256 and 100 km, respectively. The field aligned currents are taken to be constant in space and time over the grid. The plasma density n in equation (13) was advanced in time using a multi-dimensional flux-corrected variable timestep leapfrog-trapezoid scheme [Zalesak, 1979] which is second order in time and fourth order in space. At each timestep the self-consistent electrostatic potential $\delta\varphi$ of the plasma enhancement in eq. (14) was determined using a Chebychev iterative method [McDonald, 1980] with a convergence criterion of 10^{-4}. Periodic boundary conditions were imposed in the east-west direction with Neumann boundary conditions ($\partial/\partial y = 0$) in the north-south direction. A slab

approximation is used to model the zero order convecting plasma enhancements in the diffuse auroral ionosphere with the north-south profile given by $n_o(y') = N_o \{1 + 4.5 [\tanh(y'-y_1)/L + \tanh(y_2-y')/L)]\} (1 + \epsilon(x',y'))$ with $N_o = 1 \times 10^5 cm^{-3}$, $y_1 = 50$ km, and $y_2 = 125$ km. This gives a maximum plasma enhancement density to background ratio of approximately 10. The initial perturbation $\epsilon(x',y')$ has a root mean square value of 0.01 and has a radially Gaussian dependence on x' and y'. We now drop the prime notation for clarity.

4. RESULTS

In the following we consider the linear and nonlinear evolution of plasma enhancements in the diffuse auroral F region ionosphere in an approximately horizontal plane at 350 km altitude almost perpendicular to the magnetic field. We take the following typical parameters [Vickrey et al., 1980; Schunk and Walker, 1973; Banks and Kockarts, 1973] L = 20 km, $\nu_{in}/\Omega_i = 2 \times 10^{-4}$, $\nu_{ei}/\Omega_e = 2 \times 10^{-4}$, $E_{ox} = 10$ mV/m $T_e = T_i = 1000°K$ and $J_{\parallel} = 1\ \mu A/m^2$ (which gives a current velocity of $V_d \simeq 60$ m/sec with $N_o \simeq 1 \times 10^5 cm^{-3}$). In addition, we assume that the diffuse auroral particle precipitation current $J_{\parallel}$ is downward ($V_d < 0$) and spatially and temporally uniform over the entire plasma enhancement. In order to find the location and magnitude of the maximum linear growth rates to be expected with this set of parameters we first compute $\theta_m = k_{\parallel}/k_x$ as given in eq. (12) with $V_d \equiv -|V_d| = -60$ m/sec. This gives two values for θ_m which are $\theta^+ = 1.4 \times 10^{-5}$ and $\theta^- = -6.5 \times 10^{-4}$. The first value θ^+ gives a maximum linear growth rate $\gamma_{max} \simeq 1.1 \times 10^{-2} sec^{-1}$ on the poleward side ($\partial n_o/\partial y < 0$) with linearly damped perturbations $\gamma_{max} \simeq 3 \times 10^{-3} sec^{-1}$ on the equatorward side ($\partial n_o/\partial y > 0$). The second value θ^- gives only a marginally unstable growth rate of $\gamma_{max} \simeq 2.1 \times 10^{-4} sec^{-1}$ on the

equatorward side with damped fluctuations $\gamma_{max} \simeq -2.3 \times 10^{-4} sec^{-1}$ on the poleward side. These results agree with the experimental observations [Vickrey et al., 1980] that the largest linear growth rates occur on the poleward side of the convecting plasma enhancements. In this case the effect of the field-aligned currents is to enhance the $\underline{E} \times \underline{B}$ gradient-drift instability growth rate on the poleward side. The currents are too weak for the cases studied observationally to give appreciable growth on the equatorward side of the plasma enhancements. We will then consider the evolution of modes satisfying $\theta^{+} = k_{\parallel}/k_x = 1.4 \times 10^{-5}$.

We consider two models with different initial electric field configurations. Model 1 has $E_{ox} = 10$ mV/m, $E_{oy} = 0$ while Model 2 takes $E_{ox} = 8$ mV/m, $E_{oy} = 2$ mV/m. Figure 2a-2d gives the evolution of the plasma enhancement using Model 1 (no northward electric field). Figure 2a shows the initial configuration which includes the small perturbation. Figure 2b illustrates the linear regime of the simulations and shows unstable growth on the poleward side of the plasma enhancement as predicted by the linear result given by eq. (11). One can note the depletion jetting to the equatorward side of the enhancement in analogy to the initial evolution of the $\underline{E} \times \underline{B}$ gradient drift instability in artificial ionospheric plasma clouds [Zabusky et al., 1973; Scannapieco et al., 1976]. Figure 2c gives the structure of the plasma enhancement at t = 1000 sec and shows steepened fingers which are beginning to elongate. Finally Figure 2d displays the plasma enhancement at t = 1600 sec in the well-developed nonlinear regime. The poleward edges of the principal fingers (striations) have steepened, become quasi-one dimensional and bifurcated. The length scales on Figure 2a-d are distorted with the depletions longer and narrower than is depicted.

Figure 3a-b give sample one-dimensional spatial power spectra at $t = 1600$ sec both in the east-west ($P(k_x)$) and north-south ($P(k_y)$) directions respectively for Model 1. These power spectra are defined as follows

$$P(k_x) = \int dk_y \, \bar{P}(k_x,k_y)$$

and

$$P(k_y) = \int dk_x \, \bar{P}(k_x,k_y)$$

where $\bar{P}(k_x,k_y) \equiv (L_x L_y)^{-1} [\delta n(k_x,k_y)/N_o]^2$ is the spectral density, $\delta n = N-N_o$ with N_o the peak plasma enhancement density, and $L_x L_y$ is the area of the numerical simulation plane. For both cases these power spectra are well-fitted with an inverse power law with spectral index $n_x \simeq 2\text{-}2.5$ for $2\pi/k_x$ between approximately 100 and 3 km and $n_y \simeq 2$ for $2\pi/k_y$ between 256 and 3 km.

Figure 4a-4d illustrate the evolution of the plasma enhancement using Model 2 with a westward electric field $E_{ox} = 8$ mV/m together with a northward component $E_{oy} = 2$ mV/m using the same initial conditions as in the previous case ($E_{oy} = 0$) at $t = 0$, 550, 1000, and 1600 sec. As in model 1, these electric field components give two values for θ_m which are $\theta^+ = 1.7 \times 10^{-5}$ and $\theta^- = -5.03 \times 10^{-4}$. Since θ^+ gives the largest linear growth rate of $\gamma_{max} \simeq 8.0 \times 10^{-3}$ sec^{-1} on the poleward side, we consider in Model 2 those modes satisfying $\theta^+ = k_\parallel/k_x = 1.7 \times 10^{-5}$. Figure 4a gives the initial configuration which is identical to Fig. 2a. Figure 4b shows the isodensity contours of the plasmas enhancement at $t = 550$ sec where one can note a westward tilt to the fingers on the unstable poleward side and decreased depletion jetting to the equatorward side in comparison to Fig. 2b. This tilt is reminiscent of ionospheric plasma cloud structuring [Perkins and Doles, 1975] in ambient electric fields which are not initially perpendicular to the initial plasma cloud density gradient. The tilt can be explained, in part, by referring to the discussion following eq. (9) which

states that the linear growth rate maximizes away from the direction perpendicular to the initial plasma enhancement density gradient when $\underline{E} \cdot \nabla n_o \neq 0$. The decreased depletion jetting to the equatorward side of the plasma enhancement in Fig. 4b as opposed to Fig. 2b can be resolved by noting than the linear growth rate in Model 2 ($\beta \simeq 14^o$) is reduced from Model 1 ($\beta = 0$) due to the $\cos^2 (\beta/2)$ factor in eq. (10). Figure 4 c gives the structure of the plasma enhancement at t = 1000 sec for Model 2 which also appears slightly less developed than in Fig. 2c which contains no northward electric field component. Finally, Fig. 4d details the plasma enhancement at t = 1600 sec for Model 2. One notes that the eastward edge of the large finger on the westward side of the grid is slightly stepper than the westward edge ($\underline{E}_o \cdot \nabla n_o \neq 0$). This may lead to L-shell aligned east-west kilometer size structures due to secondary $\underline{E} \times \underline{B}$ instabilities although the present simulations do not have adequate spatial resolution to develop such an hypothesis. In addition, there is more pronounced bending of the fingers in Fig. 4d in comparison to Fig. 2d and less bifurcation on the poleward tips of the striations. As mentioned previously, these features can be explained, in part, by the small northward electric field components.

Figure 5a-b give the one-dimensional east-west $P(k_x)$ and north-south $P(k_y)$ spatial power spectra at t = 1600 sec for Model 2. The power laws and spectral indices are similar to Model 1.

5. SUMMARY AND DISCUSSION

We have studied, through numerical simulations, the nonlinear evolution of plasma enhancements in the diffuse auroral F region ionosphere. We have

shown that equatorward convecting plasma slabs initially limited in latitudinal extent can be destabilized on the poleward sides by a combination of the effects of convection and field aligned currents. These simulations indicate that this destabilization leads to striation-like structures (elongated in the north-south direction) which can form and cascade from long wavelengths ($\sim$ 100 km) to shorter scale sizes ($\sim$ 1 km) on the order of an hour. The one-dimensional irregularity spatial power spectra in the east-west direction $P(k_x) \propto k_x^{-n_x}$, $n_x \simeq 2$-2.5, for $2\pi/k_x$ between 100 km and 3 km while in the north-south direction $P(k_y) \propto k_y^{-n_y}$, $n_y \simeq 2$, for $2\pi/k_y$ between 256 km and 3 km.

In this paper we have studied the quasi-two dimensional linear and nonlinear evolution of models of plasma enhancements in the diffuse auroral F region ionosphere. This has been accomplished by solving the plasma fluid equations in a horizontal plane approximately perpendicular to the magnetic field. The observed plasma enhancements are three dimensional [Vickrey et al., 1980]. However the horizontal gradients are much steeper than the vertical denstiy gradients allowing one to approximately model the plasma enhancements by vertical slabs. In addition, we have not included a full spectrum of finite $k_\parallel$ modes in these simulations. However, since the modes with maximum linear growth rate have $k_\parallel/k_\perp \ll 1$, the important structuring processes will occur in the plane nearly perpendicular to the magnetic field.

Finally, we note that we have not addressed the source mechanism of the plasma enhancements, their coupling to other levels, e.g., E-region, the nature of the intermediate wavelength irregularities ($\lambda \sim 1$ km) in the plasma enhancements, and the role of neutral winds. These topics will be discussed in future studies.

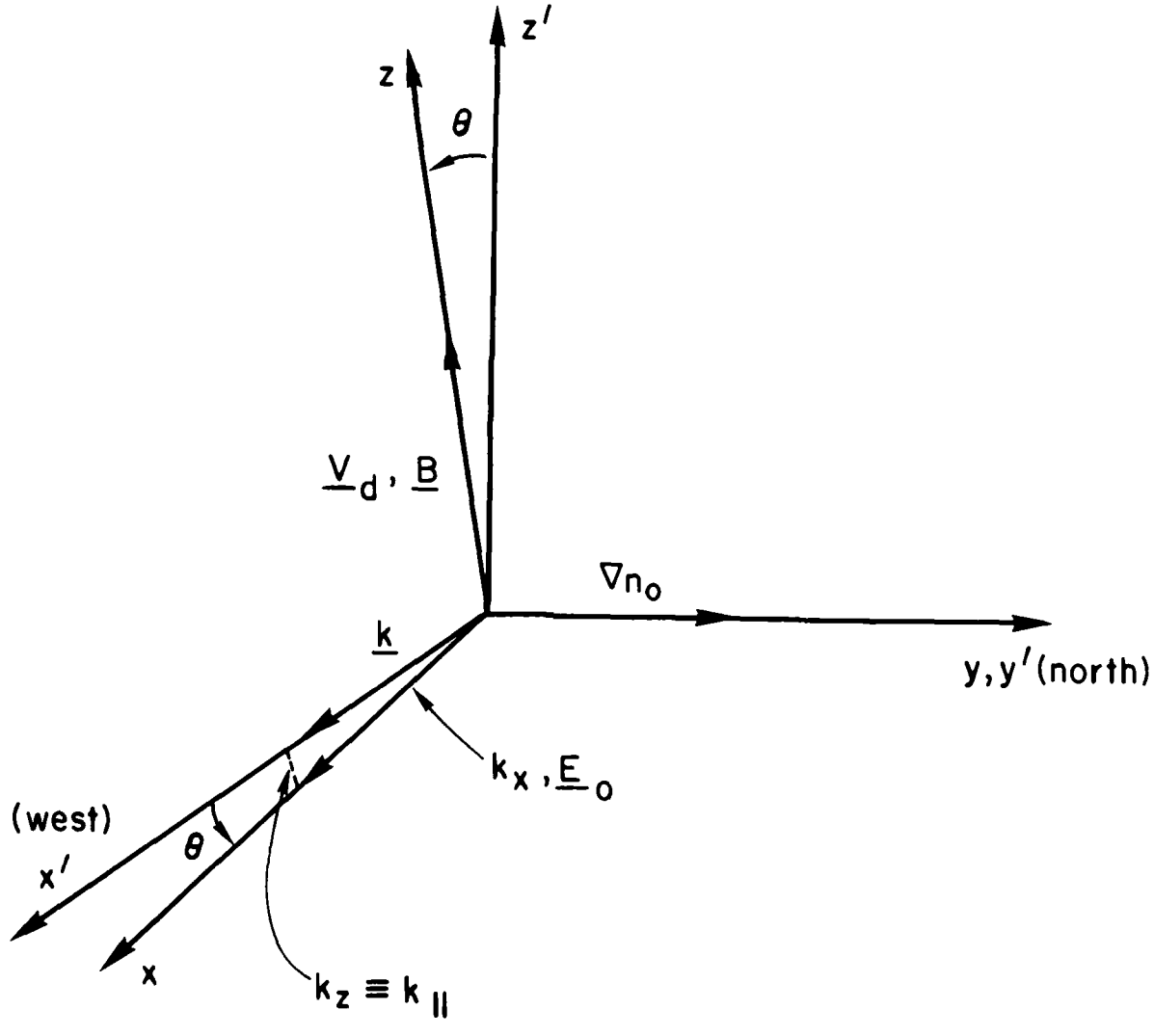

Fig. 1 — Coordinate system used in simulations. The x'y' is the simulation plane. The x',x,z',z axes are coplanar.

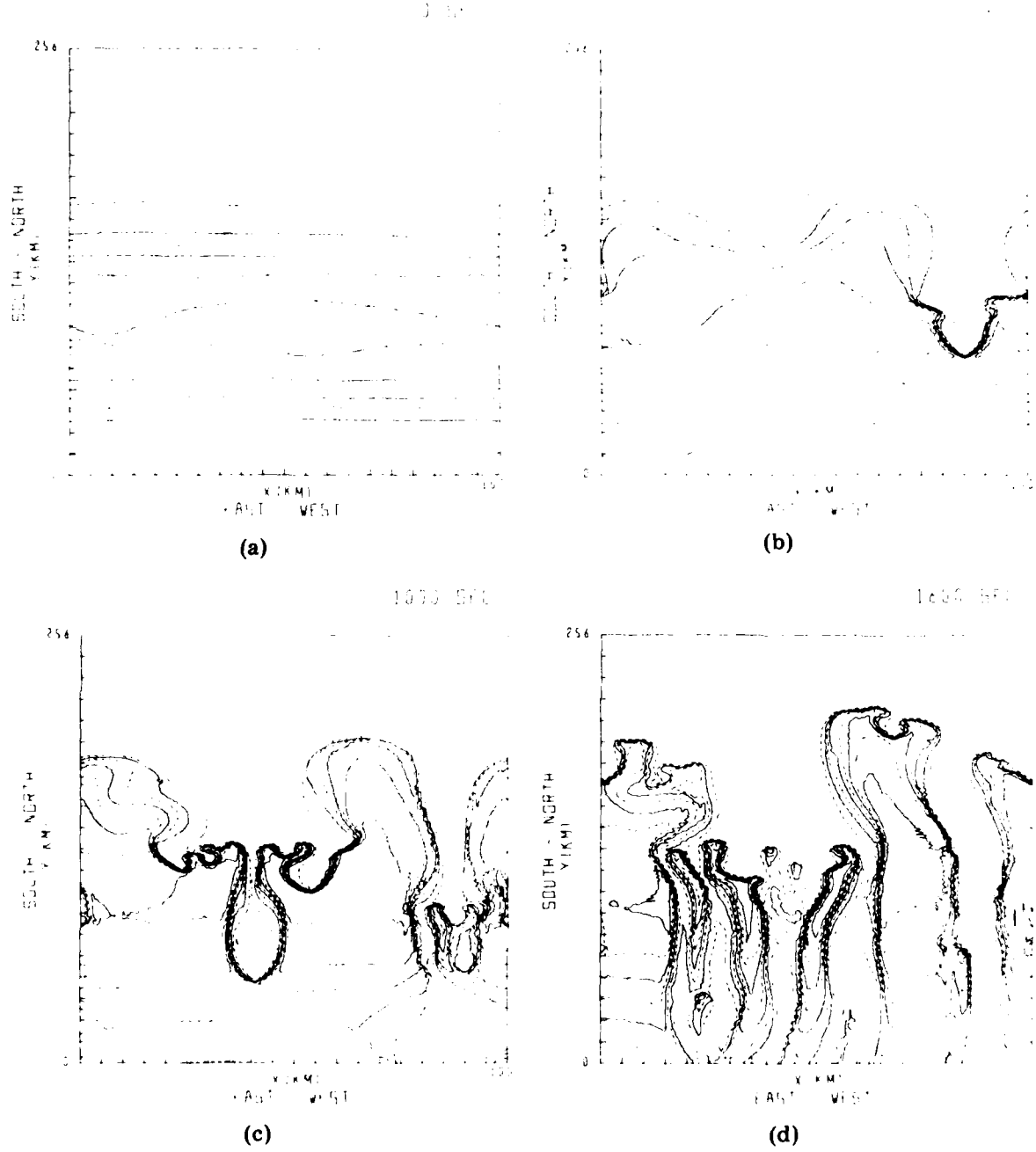

Fig. 2 — Real space isodensity contour plots of $n(x',y')/N_o$ for model 1 at (a) t = 0 sec, (b) t = 550 sec, (c) t = 1000 sec, (d) t = 1600 sec. The y-axis is compressed by a factor of 2.58. The distance between tic marks in the x-direction (y-direction) is 5 km (12.8 km). Eight contours are plotted in equal increments of 1.25 beginning at 1.25. The observer is looking upward along the magnetic field lines.

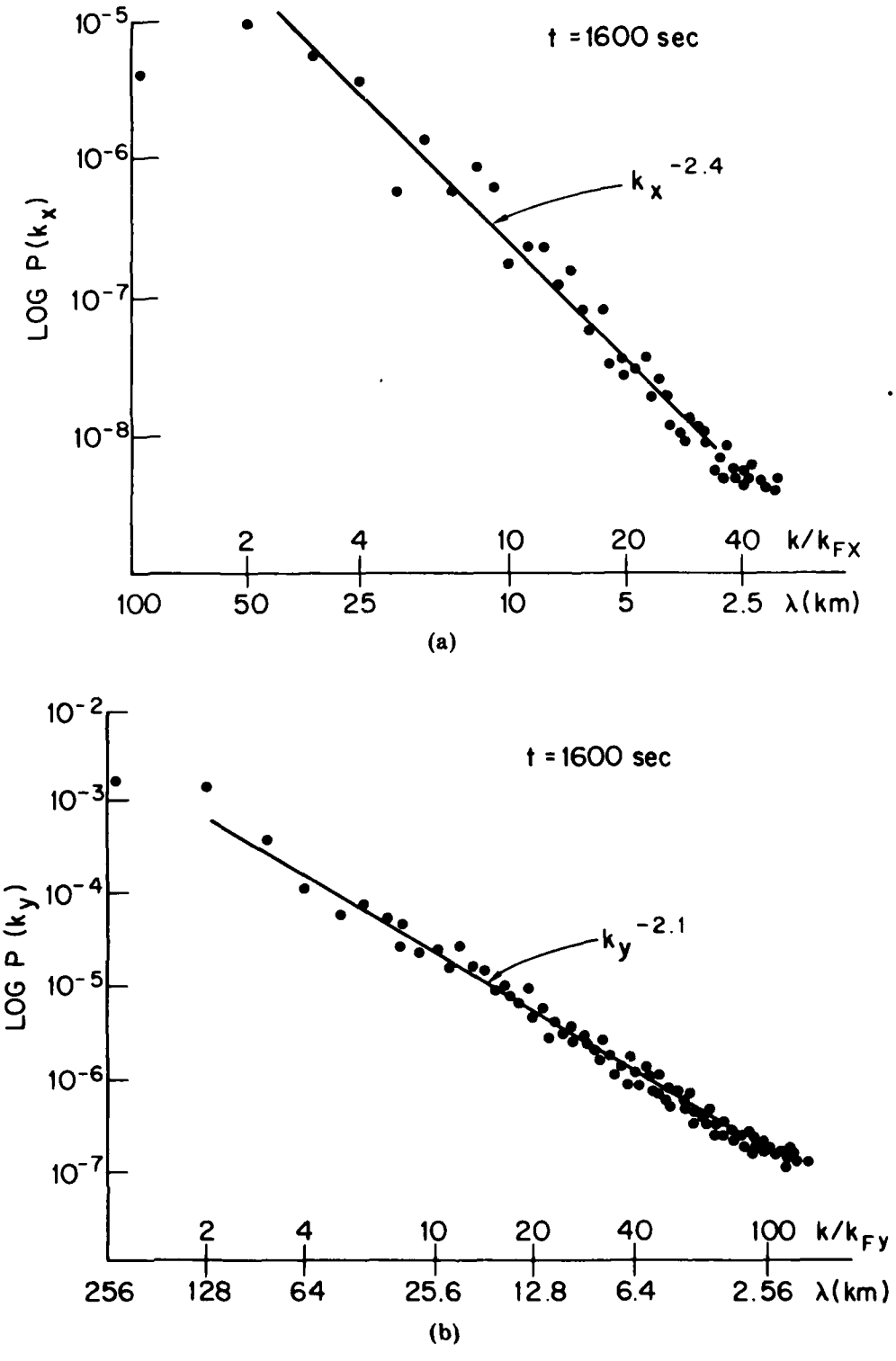

Fig. 3 — One dimensional (a) x power spectra $P(k_x)$ and (b) y power spectra $P(k_y)$ at t = 1600 sec for model 1. In (a) $k_{Fx} = 2\pi/100$ km^{-1} while in (b) $k_{Fy} = 2\pi/256$ km^{-1}. The dots represent the numerical simulation results; the solid curve is a least squares fit to modes 2-30 in the x-direction and to modes 2-80 in the y-direction. The units of $P(k_x)$, $P(k_y)$ are km.

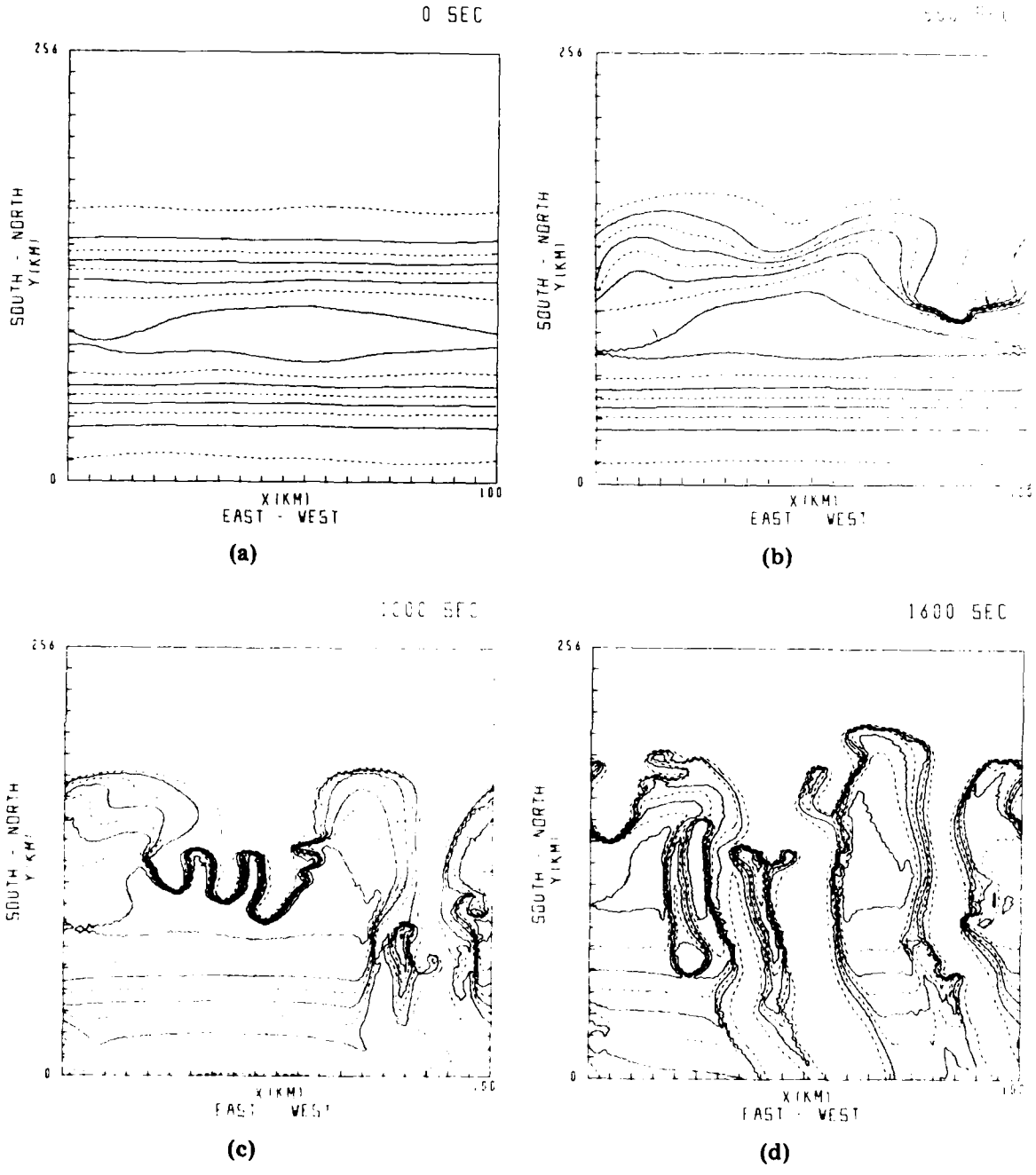

Fig. 4 — Real space isodensity contour plots of $n(x',y')/N_o$ for model 2 at (a) t = 0 sec, (b) t = 550 sec, (c) t = 1000 sec, (d) t = 1600 sec using the same format as Fig. 2.

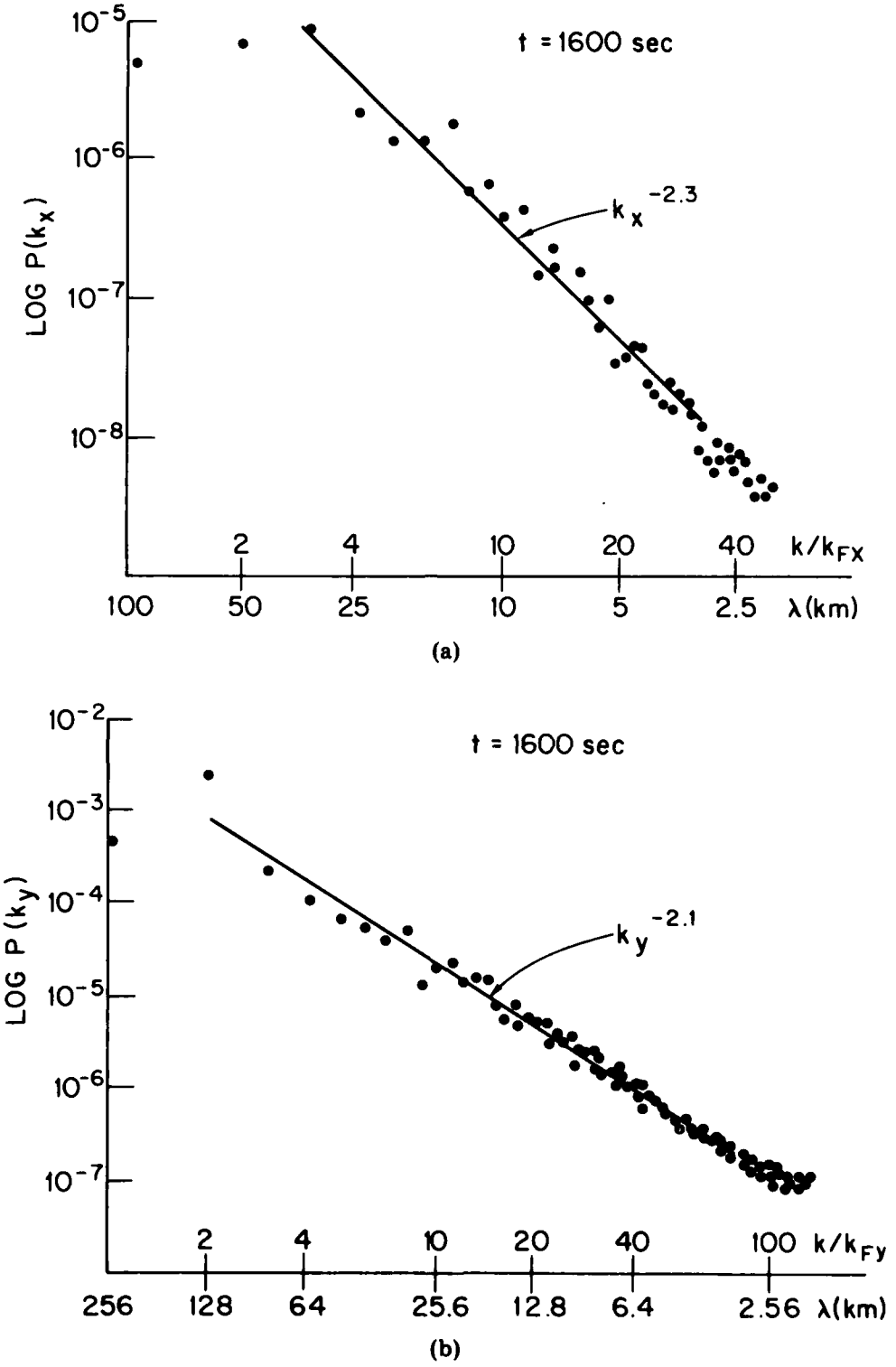

Fig. 5 — One-dimensional (a) x-power spectra $P(k_x)$ and (b) y-power spectra $P(k_y)$ at t = 1600 sec for model 2 in same format as Fig. 3.

ACKNOWLEDGEMENTS

We wish to thank J.F. Vickrey, and C.L. Rino for useful discussions. This work was supported by the Defense Nuclear Agency and the Office of Naval Research.

REFERENCES

Banks, P.M. and G. Kockarts, Aeronomy Part A (Academic Press, Inc., New York, NY, 1973).

Chaturvedi, P.K. and S.L. Ossakow, Nonlinear stabilization of the current convective instability in the diffuse aurora, Geophys. Res. Lett., 6, 957, 1979.

Fremouw, E.J., C.L. Rino, R.C. Livingston, and M.C. Cousins, A persistent subauroral scintillation enhancement observed in Alaska, Geophys. Res. Lett., 4, 539, 1977.

Kadomtsev, B.B. and A.V. Nedospasov, Instability of the positive column in a magnetic field and the "anomalous diffusion effect," J. Nucl. Energy, Part C, 1, 230, 1960.

Keskinen, M.J., S.L. Ossakow, and B.E. McDonald, Nonlinear evolution of diffuse auroral F region ionospheric irregularities, Geophys. Res. Lett., 7, 573, 1980.

Lee, W.W. and H. Okuda, Anomalous transport and stabilization of collisionless drift-wave instabilities, Phys. Rev. Lett., 36, 870, 1976.

Lehnert, B., Diffusion processes in the positive column in a longitudinal magnetic field, in Proceedings of the Second Geneva Conference on the Peaceful Uses of Atomic Energy, 32, 349, 1958.

Linson, L.M. and J.B. Workman, Formation of striations in ionospheric plasma clouds, J. Geophys. Res., 75, 3211, 1970.

Matsuda, Y. and H. Okuda, Simulation of dissipative trapped-electron instability in linear geometry, Phys. Rev. Lett., 36, 474, 1976.

McDonald, B.E., The Chebychev method for solving nonself-adjoint elliptic equations on a vector computer, J. Comput. Phys. 35, 147, 1980.

Ossakow, S.L. and P.K. Chaturvedi, Current convective instability in the diffuse aurora, Geophys. Res. Lett., 6, 332, 1979.

Perkins, F.W. and J.H. Doles III, Velocity shear and the E x B instability, J. Geophys. Res., 80, 211, 1975.

Rino, C.L., R.C. Livingston, and S.J. Matthews, Evidence for sheet-like auroral ionospheric irregularities, Geophys. Res. Letts., 5, 1039, 1978.

Rino, C.L. and S.J. Matthews, On the morphology of auroral-zone radiowave scintillation, J. Geophys. Res., 85, 4139, 1979.

Rino, C.L. and J. Owen, The structure of localized nighttime auroral-zone scintillation enhancements, J. Geophys. Res., 85, 2941, 1980.

Scannapieco, A.J., S.L. Ossakow, S.R. Goldman, and J.M. Pierre, Plasma cloud late time striation spectra, J. Geophys. Res., 81, 6037, 1976.

Schunk, R.W. and J.C.G. Walker, Theoretical ion densities in the lower atmosphere, Planet. Space Sci., 21, 1975, 1973.

Simon, A., Instability of a partially ionized plasma in crossed electric and magnetic fields, Phys. Fluids, 6, 382, 1963.

Vickrey, J.F., C.L. Rino, and T.A. Potemra, Chatanika/Triad observations of unstable ionization enhancements in the auroral F-region, Geophys. Res. Lett., 7, 789, 1980.

Zabusky, N.J., J.H. Doles III, and F.W. Perkins, Deformation and striation of plasma clouds in the ionosphere, 2, Numerical simulation of a non-linear two-dimensional model, J. Geophys. Res., 78, 711, 1973.

Zalesak, S.T., Fully multidimensional flux-corrected transport algorithms for fluids, J. Comp. Phys., 31, 335, 1979.

DISTRIBUTION LIST

DEPARTMENT OF DEFENSE

ASSISTANT SECRETARY OF DEFENSE
COMM, CMD, CONT & INTELL
WASHINGTON, D.C. 20301
01CY ATTN J. BABCOCK
01CY ATTN M. EPSTEIN

DIRECTOR
COMMAND CONTROL TECHNICAL CENTER
PENTAGON RM BE 685
WASHINGTON, D.C. 20301
01CY ATTN C-650
01CY ATTN C-312 R. MASON

DIRECTOR
DEFENSE ADVANCED RSCH PROJ AGENCY
ARCHITECT BUILDING
1400 WILSON BLVD.
ARLINGTON, VA. 22209
01CY ATTN NUCLEAR MONITORING RESEARCH
01CY ATTN STRATEGIC TECH OFFICE

DEFENSE COMMUNICATION ENGINEER CENTER
1860 WIEHLE AVENUE
RESTON, VA. 22090
01CY ATTN CODE R820
01CY ATTN CODE R410 JAMES W. MCLEAN
01CY ATTN CODE R720 J. WORTHINGTON

DIRECTOR
DEFENSE COMMUNICATIONS AGENCY
WASHINGTON, D.C. 20305
(ADR CNMDI: ATTN CODE 240 FOR)
01CY ATTN CODE 101B

DEFENSE TECHNICAL INFORMATION CENTER
CAMERON STATION
ALEXANDRIA, VA. 22314
(12 COPIES IF OPEN PUBLICATION, OTHERWISE 2 COPIES)
12CY ATTN TC

DIRECTOR
DEFENSE INTELLIGENCE AGENCY
WASHINGTON, D.C. 20301
01CY ATTN DT-1B
01CY ATTN DB-4C E. O'FARRELL
01CY ATTN DIAAP A. WISE
01CY ATTN DIAST-5
01CY ATTN DT-1BZ R. MORTON
01CY ATTN HQ-TR J. STEWART
01CY ATTN W. WITTIG DC-7D

DIRECTOR
DEFENSE NUCLEAR AGENCY
WASHINGTON, D.C. 20305
01CY ATTN STVL
04CY ATTN TITL
01CY ATTN DDST
03CY ATTN RAAE

COMMANDER
FIELD COMMAND
DEFENSE NUCLEAR AGENCY
KIRTLAND AFB, NM 87115
01CY ATTN FCPR

DIRECTOR
INTERSERVICE NUCLEAR WEAPONS SCHOOL
KIRTLAND AFB, NM 87115
01CY ATTN DOCUMENT CONTROL

JOINT CHIEFS OF STAFF
WASHINGTON, D.C. 20301
01CY ATTN C3S EVALUATION OFFICE

DIRECTOR
JOINT STRAT TGT PLANNING STAFF
OFFUTT AFB
OMAHA, NB 68113
01CY ATTN JLTW-2
01CY ATTN JPST G. GOETZ

CHIEF
LIVERMORE DIVISION FLD COMMAND DNA
DEPARTMENT OF DEFENSE
LAWRENCE LIVERMORE LABORATORY
P. O. BOX 808
LIVERMORE, CA 94550
01CY ATTN FCPRL

DIRECTOR
NATIONAL SECURITY AGENCY
DEPARTMENT OF DEFENSE
FT. GEORGE G. MEADE, MD 20755
01CY ATTN JOHN SKILLMAN R52
01CY ATTN FRANK LEONARD
01CY ATTN W14 PAT CLARK
01CY ATTN OLIVER H. BARTLETT W32
01CY ATTN R5

COMMANDANT
NATO SCHOOL (SHAPE)
APO NEW YORK 09172
01CY ATTN U.S. DOCUMENTS OFFICER

UNDER SECY OF DEF FOR RSCH & ENGRG
DEPARTMENT OF DEFENSE
WASHINGTON, D.C. 20301
01CY ATTN STRATEGIC & SPACE SYSTEMS (OS)

WWMCCS SYSTEM ENGINEERING ORG
WASHINGTON, D.C. 20305
01CY ATTN R. CRAWFORD

COMMANDER/DIRECTOR
ATMOSPHERIC SCIENCES LABORATORY
U.S. ARMY ELECTRONICS COMMAND
WHITE SANDS MISSILE RANGE, NM 88002
01CY ATTN DELAS-EO F. NILES

DIRECTOR
BMD ADVANCED TECH CTR
HUNTSVILLE OFFICE
P. O. BOX 1500
HUNTSVILLE, AL 35807
01CY ATTN ATC-T MELVIN T. CAPPS
01CY ATTN ATC-O W. DAVIES
01CY ATTN ATC-R DON RUSS

PROGRAM MANAGER
BMD PROGRAM OFFICE
5001 EISENHOWER AVENUE
ALEXANDRIA, VA 22333
01CY ATTN DACS-BMT J. SHEA

CHIEF C-E SERVICES DIVISION
U.S. ARMY COMMUNICATIONS CMD
PENTAGON RM 1B269
WASHINGTON, D.C. 20310
01CY ATTN C-E-SERVICES DIVISION

COMMANDER
FRADCOM TECHNICAL SUPPORT ACTIVITY
DEPARTMENT OF THE ARMY
FORT MONMOUTH, N.J. 07703
01CY ATTN DRSEL-NL-RD H. BENNET
01CY ATTN DRSEL-PL-ENV H. BOMKE
01CY ATTN J. E. QUIGLEY

COMMANDER
HARRY DIAMOND LABORATORIES
DEPARTMENT OF THE ARMY
2800 POWDER MILL ROAD
ADELPHI, MD 20783
(CNWDI-INNER ENVELOPE: ATTN: DELHD-RBH)
01CY ATTN DELHD-TI M. WEINER
01CY ATTN DELHD-RB R. WILLIAMS
01CY ATTN DELHD-NP F. WIMENITZ
01CY ATTN DELHD-NP C. MOAZED

COMMANDER
U.S. ARMY COMM-ELEC ENGRG INSTAL AGY
FT. HUACHUCA, AZ 85613
01CY ATTN CCC-EMEO GEORGE LANE

COMMANDER
U.S. ARMY FOREIGN SCIENCE & TECH CTR
220 7TH STREET, NE
CHARLOTTESVILLE, VA 22901
01CY ATTN DRXST-SD
01CY ATTN R. JONES

COMMANDER
U.S. ARMY MATERIEL DEV & READINESS CMD
5001 EISENHOWER AVENUE
ALEXANDRIA, VA 22333
01CY ATTN DRCLDC J. A. BENDER

COMMANDER
U.S. ARMY NUCLEAR AND CHEMICAL AGENCY
7500 BACKLICK ROAD
BLDG 2073
SPRINGFIELD, VA 22150
01CY ATTN LIBRARY

DIRECTOR
U.S. ARMY BALLISTIC RESEARCH LABS
ABERDEEN PROVING GROUND, MD 21005
01CY ATTN TECH LIB EDWARD BAICY

COMMANDER
U.S. ARMY SATCOM AGENCY
FT. MONMOUTH, NJ 07703
01CY ATTN DOCUMENT CONTROL

COMMANDER
U.S. ARMY MISSILE INTELLIGENCE AGENCY
REDSTONE ARSENAL, AL 35809
01CY ATTN JIM GAMBLE

DIRECTOR
U.S. ARMY TRADOC SYSTEMS ANALYSIS ACTIVITY
WHITE SANDS MISSILE RANGE, NM 88002
01CY ATTN ATAA-SA
01CY ATTN TCC/F. PAYAN JR.
01CY ATTN ATAA-TAC LTC J. HESSE

COMMANDER
NAVAL ELECTRONIC SYSTEMS COMMAND
WASHINGTON, D.C. 20360
01CY ATTN NAVALEX 034 T. HUGHES
01CY ATTN PME 117
01CY ATTN PME 117-T
01CY ATTN CODE 5011

COMMANDING OFFICER
NAVAL INTELLIGENCE SUPPORT CTR
4301 SUITLAND ROAD, BLDG. 5
WASHINGTON, D.C. 20390
01CY ATTN MR. DUBBIN STIC 12
01CY ATTN NISC-50
01CY ATTN CODE 5404 J. GALET

COMMANDER
NAVAL OCEAN SYSTEMS CENTER
SAN DIEGO, CA 92152
03CY ATTN CODE 532 W. MOLER
01CY ATTN CODE 0230 C. BAGGETT
01CY ATTN CODE 81 K. EASTMAN

DIRECTOR
NAVAL RESEARCH LABORATORY
WASHINGTON, D.C. 20375
01CY ATTN CODE 4700 T. P. COFFEY (26 CYS IF UN, 1 CY IF CLASS)
01CY ATTN CODE 4701 JACK D. BROWN
01CY ATTN CODE 4780 BRANCH HEAD (150 CYS IF UN, 1 CY IF CLASS)
01CY ATTN CODE 7500
01CY ATTN CODE 7550
01CY ATTN CODE 7580
01CY ATTN CODE 7551
01CY ATTN CODE 7555
01CY ATTN CODE 4730 E. MCLEAN
01CY ATTN CODE 4187

COMMANDER
NAVAL SEA SYSTEMS COMMAND
WASHINGTON, D.C. 20362
01CY ATTN CAPT R. PITKIN

COMMANDER
NAVAL SPACE SURVEILLANCE SYSTEM
DAHLGREN, VA 22448
01CY ATTN CAPT J. H. BURTON

OFFICER-IN-CHARGE
NAVAL SURFACE WEAPONS CENTER
WHITE OAK, SILVER SPRING, MD 20910
01CY ATTN CODE F31

DIRECTOR
STRATEGIC SYSTEMS PROJECT OFFICE
DEPARTMENT OF THE NAVY
WASHINGTON, D.C. 20376
01CY ATTN NSP-2141
01CY ATTN NSSP-2722 FRED WIMBERLY

COMMANDER
NAVAL SURFACE WEAPONS CENTER
DAHLGREN LABORATORY
DAHLGREN, VA 22448
01CY ATTN CODE DF-14 R. BUTLER

OFFICE OF NAVAL RESEARCH
ARLINGTON, VA 22217
01CY ATTN CODE 465
01CY ATTN CODE 461
01CY ATTN CODE 402
01CY ATTN CODE 420
01CY ATTN CODE 421

COMMANDER
AEROSPACE DEFENSE COMMAND/DC
DEPARTMENT OF THE AIR FORCE
ENT AFB, CO 80912
01CY ATTN DC MR. LONG

COMMANDER
AEROSPACE DEFENSE COMMAND/XPD
DEPARTMENT OF THE AIR FORCE
ENT AFB, CO 80912
01CY ATTN XPDQQ
01CY ATTN XP

AIR FORCE GEOPHYSICS LABORATORY
HANSCOM AFB, MA 01731
01CY ATTN OPR HAROLD GARDNER
01CY ATTN OPR-1 JAMES C. ULWICK
01CY ATTN LKB KENNETH S. W. CHAMPION
01CY ATTN OPR ALVA T. STAIR
01CY ATTN PHP JULES AARONS
01CY ATTN PHD JURGEN BUCHAU
01CY ATTN PHD JOHN P. MULLEN

AF WEAPONS LABORATORY
KIRTLAND AFB, NM 87117
01CY ATTN SUL
01CY ATTN CA ARTHUR H. GUENTHER
01CY ATTN NTYC 1LT G. KRAJCI

AFTAC
PATRICK AFB, FL 32925
01CY ATTN TF/MAJ WILEY
01CY ATTN TN

AIR FORCE AVIONICS LABORATORY
WRIGHT-PATTERSON AFB, OH 45433
01CY ATTN AAD WADE HUNT
01CY ATTN AAD ALLEN JOHNSON

DEPUTY CHIEF OF STAFF
RESEARCH, DEVELOPMENT, & ACQ
DEPARTMENT OF THE AIR FORCE
WASHINGTON, D.C. 20330
01CY ATTN AFRDQ

HEADQUARTERS
ELECTRONIC SYSTEMS DIVISION/XR
DEPARTMENT OF THE AIR FORCE
HANSCOM AFB, MA 01731
01CY ATTN XR J. DEAS

HEADQUARTERS
ELECTRONIC SYSTEMS DIVISION/YSEA
DEPARTMENT OF THE AIR FORCE
HANSCOM AFB, MA 01732
01CY ATTN YSEA

HEADQUARTERS
ELECTRONIC SYSTEMS DIVISION/DC
DEPARTMENT OF THE AIR FORCE
HANSCOM AFB, MA 01731
01CY ATTN DCKC MAJ J.L. CLARK

COMMANDER
FOREIGN TECHNOLOGY DIVISION, AFSC
WRIGHT-PATTERSON AFB, OH 45433
01CY ATTN NICD LIBRARY
01CY ATTN ETDP B. BALLARD

COMMANDER
ROME AIR DEVELOPMENT CENTER, AFSC
GRIFFISS AFB, NY 13441
01CY ATTN DOC LIBRARY/TSLD
01CY ATTN OCSE V. COYNE

SAMSO/SZ
POST OFFICE BOX 92960
WORLDWAY POSTAL CENTER
LOS ANGELES, CA 90009
(SPACE DEFENSE SYSTEMS)
01CY ATTN SZJ

STRATEGIC AIR COMMAND/XPFS
OFFUTT AFB, NB 68113
01CY ATTN XPFS MAJ B. STEPHAN
01CY ATTN ADWATE MAJ BRUCE BAUER
01CY ATTN NRT
01CY ATTN DOK CHIEF SCIENTIST

SAMSO/SK
P. O. BOX 92960
WORLDWAY POSTAL CENTER
LOS ANGELES, CA 90009
01CY ATTN SKA (SPACE COMM SYSTEMS) M. CLAVIN

SAMSO/MN
NORTON AFB, CA 92409
(MINUTEMAN)
01CY ATTN MNNL LTC KENNEDY

COMMANDER
ROME AIR DEVELOPMENT CENTER, AFSC
HANSCOM AFB, MA 01731
01CY ATTN EEP A. LORENTZEN

DEPARTMENT OF ENERGY
ALBUQUERQUE OPERATIONS OFFICE
P. O. BOX 5400
ALBUQUERQUE, NM 87115
01CY ATTN DOC CON FOR D. SHERWOOD

DEPARTMENT OF ENERGY
LIBRARY ROOM G-042
WASHINGTON, D.C. 20545
01CY ATTN DOC CON FOR A. LABOWITZ

EG&G, INC.
LOS ALAMOS DIVISION
P. O. BOX 809
LOS ALAMOS, NM 85544
01CY ATTN DOC CON FOR J. BREEDLOVE

UNIVERSITY OF CALIFORNIA
LAWRENCE LIVERMORE LABORATORY
P. O. BOX 808
LIVERMORE, CA 94550
01CY ATTN DOC CON FOR TECH INFO DEPT
01CY ATTN DOC CON FOR L-389 R. OTT
01CY ATTN DOC CON FOR L-31 R. HAGER
01CY ATTN DOC CON FOR L-46 F. SEWARD

LOS ALAMOS SCIENTIFIC LABORATORY
P. O. BOX 1663
LOS ALAMOS, NM 87545
01CY ATTN DOC CON FOR J. WOLCOTT
01CY ATTN DOC CON FOR R. F. TASCHEK
01CY ATTN DOC CON FOR E. JONES
01CY ATTN DOC CON FOR J. MALIK
01CY ATTN DOC CON FOR R. JEFFRIES
01CY ATTN DOC CON FOR J. ZINN
01CY ATTN DOC CON FOR P. KEATON
01CY ATTN DOC CON FOR D. WESTERVELT

SANDIA LABORATORIES
P. O. BOX 5800
ALBUQUERQUE, NM 87115
01CY ATTN DOC CON FOR W. BROWN
01CY ATTN DOC CON FOR A. THORNBROUGH
01CY ATTN DOC CON FOR T. WRIGHT
01CY ATTN DOC CON FOR D. DAHLGREN
01CY ATTN DOC CON FOR 3141
01CY ATTN DOC CON FOR SPACE PROJECT DIV

SANDIA LABORATORIES
LIVERMORE LABORATORY
P. O. BOX 969
LIVERMORE, CA 94550
01CY ATTN DOC CON FOR B. MURPHEY
01CY ATTN DOC CON FOR T. COOK

OFFICE OF MILITARY APPLICATION
DEPARTMENT OF ENERGY
WASHINGTON, D.C. 20545
01CY ATTN DOC CON FOR Dr. Yo Song

OTHER GOVERNMENT

CENTRAL INTELLIGENCE AGENCY
ATTN RD/SI, RM 5G48, HQ BLDG
WASHINGTON, D.C. 20505
01CY ATTN OSI/PSID RM 5F 19

DEPARTMENT OF COMMERCE
NATIONAL BUREAU OF STANDARDS
WASHINGTON, D.C. 20234
(ALL CORRES: ATTN SEC OFFICER FOR)
01CY ATTN R. MOORE

INSTITUTE FOR TELECOM SCIENCES
NATIONAL TELECOMMUNICATIONS & INFO ADMIN
BOULDER, CO 80303
01CY ATTN A. JEAN (UNCLASS ONLY)
01CY ATTN W. UTLAUT
01CY ATTN D. CROMBIE
01CY ATTN L. BERRY

NATIONAL OCEANIC & ATMOSPHERIC ADMIN
ENVIRONMENTAL RESEARCH LABORATORIES
DEPARTMENT OF COMMERCE
BOULDER, CO 80302
01CY ATTN R. GRUBB
01CY ATTN AERONOMY LAB G. REID

DEPARTMENT OF DEFENSE CONTRACTORS

AEROSPACE CORPORATION
P. O. Box 92957
LOS ANGELES, CA 90009
01CY ATTN I. GARFUNKEL
01CY ATTN T. SALMI
01CY ATTN V. JOSEPHSON
01CY ATTN S. BOWER
01CY ATTN N. STOCKWELL
01CY ATTN D. OLSEN

ANALYTICAL SYSTEMS ENGINEERING CORP
5 OLD CONCORD ROAD
BURLINGTON, MA 01803
01CY ATTN RADIO SCIENCES

BERKELEY RESEARCH ASSOCIATES, INC.
P. O. BOX 983
BERKELEY, CA 94701
01CY ATTN J. WORKMAN

BOEING COMPANY, THE
P. O. BOX 3707
SEATTLE, WA 98124
01CY ATTN G. KEISTER
01CY ATTN D. MURRAY
01CY ATTN G. HALL
01CY ATTN J. KENNEY

CALIFORNIA AT SAN DIEGO, UNIV OF
P.O. Box 6049
SAN DIEGO, CA 92106

BROWN ENGINEERING COMPANY, INC.
CUMMINGS RESEARCH PARK
HUNTSVILLE, AL 35807
01CY ATTN ROMEO A. DELIBERIS

CHARLES STARK DRAPER LABORATORY, INC.
555 TECHNOLOGY SQUARE
CAMBRIDGE, MA 02139
01CY ATTN D. B. COX
01CY ATTN J. P. GILMORE

COMSAT LABORATORIES
LINTHICUM ROAD
CLARKSBURG, MD 20734
01CY ATTN G. HYDE

CORNELL UNIVERSITY
DEPARTMENT OF ELECTRICAL ENGINEERING
ITHACA, NY 14850
01CY ATTN D. T. FARLEY JR

ELECTROSPACE SYSTEMS, INC.
BOX 1359
RICHARDSON, TX 75080
01CY ATTN H. LOGSTON
01CY ATTN SECURITY (PAUL PHILLIPS)

ESL INC.
495 JAVA DRIVE
SUNNYVALE, CA 94086
01CY ATTN J. ROBERTS
01CY ATTN JAMES MARSHALL
01CY ATTN C. W. PRETTIE

GENERAL ELECTRIC COMPANY
SPACE DIVISION
VALLEY FORGE SPACE CENTER
GODDARD BLVD KING OF PRUSSIA
P. O. BOX 8555
PHILADELPHIA, PA 19101
01CY ATTN M. H. BORTNER SPACE SCI LAB

GENERAL ELECTRIC COMPANY
P. O. BOX 1122
SYRACUSE, NY 13201
01CY ATTN F. REIBERT

GENERAL ELECTRIC COMPANY
TEMPO-CENTER FOR ADVANCED STUDIES
816 STATE STREET (P.O. DRAWER QQ)
SANTA BARBARA, CA 93102
01CY ATTN DASIAC
01CY ATTN DON CHANDLER
01CY ATTN TOM BARRETT
01CY ATTN TIM STEPHANS
01CY ATTN WARREN S. KNAPP
01CY ATTN WILLIAM MCNAMARA
01CY ATTN B. GAMBILL
01CY ATTN MACK STANTON

GENERAL ELECTRIC TECH SERVICES CO., INC.
HMES
COURT STREET
SYRACUSE, NY 13201
01CY ATTN G. MILLMAN

GENERAL RESEARCH CORPORATION
SANTA BARBARA DIVISION
P. O. BOX 6770
SANTA BARBARA, CA 93111
01CY ATTN JOHN ISE JR
01CY ATTN JOEL GARBARINO

GEOPHYSICAL INSTITUTE
UNIVERSITY OF ALASKA
FAIRBANKS, AK 99701
(ALL CLASS ATTN: SECURITY OFFICER)
01CY ATTN T. N. DAVIS (UNCL ONLY)
01CY ATTN NEAL BROWN (UNCL ONLY)
01CY ATTN TECHNICAL LIBRARY

GTE SYLVANIA, INC.
ELECTRONICS SYSTEMS GRP-EASTERN DIV
77 A STREET
NEEDHAM, MA 02194
01CY ATTN MARSHAL CROSS

ILLINOIS, UNIVERSITY OF
107 COBLE HALL
150 DAVENPORT HOUSE
CHAMPAIGN, IL 61820
(ALL CORRES ATTN DAN MCCLELLAND)
01CY FOR K. YEH

INSTITUTE FOR DEFENSE ANALYSES
400 ARMY-NAVY DRIVE
ARLINGTON, VA 22202
01CY ATTN J. M. AEIN
01CY ATTN ERNEST BAUER
01CY ATTN HANS WOLFHARD
01CY ATTN JOEL BENGSTON

HSS, INC.
2 ALFRED CIRCLE
BEDFORD, MA 01730
01CY ATTN DONALD HANSEN

INTL TEL & TELEGRAPH CORPORATION
500 WASHINGTON AVENUE
NUTLEY, NJ 07110
01CY ATTN TECHNICAL LIBRARY

JAYCOR
1401 CAMINO DEL MAR
DEL MAR, CA 92014
01CY ATTN S. R. GOLDMAN

JOHNS HOPKINS UNIVERSITY
APPLIED PHYSICS LABORATORY
JOHNS HOPKINS ROAD
LAUREL, MD 20810
01CY ATTN DOCUMENT LIBRARIAN
01CY ATTN THOMAS POTEMRA
01CY ATTN JOHN DASSOULAS

LOCKHEED MISSILES & SPACE CO INC
P. O. BOX 504
SUNNYVALE, CA 94088
01CY ATTN DEPT 60-12
01CY ATTN D. R. CHURCHILL

LOCKHEED MISSILES AND SPACE CO INC
3251 HANOVER STREET
PALO ALTO, CA 94304
01CY ATTN MARTIN WALT DEPT 52-10
01CY ATTN RICHARD G. JOHNSON DEPT 52-12
01CY ATTN W. L. IMHOF DEPT 52-12

KAMAN SCIENCES CORP
P. O. BOX 7463
COLORADO SPRINGS, CO 80933
01CY ATTN T. MEAGHER

LINKABIT CORP
10453 ROSELLE
SAN DIEGO, CA 92121
01CY ATTN IRWIN JACOBS

M.I.T. LINCOLN LABORATORY
P. O. BOX 73
LEXINGTON, MA 02173
01CY ATTN DAVID M. TOWLE
01CY ATTN P. WALDRON
01CY ATTN L. LOUGHLIN
01CY ATTN D. CLARK

MARTIN MARIETTA CORP
ORLANDO DIVISION
P. O. BOX 5837
ORLANDO, FL 32805
01CY ATTN R. HEFFNER

PHYSICAL DYNAMICS INC.
P. O. BOX 3027
BELLEVUE, WA 98009
01CY ATTN E. J. FREMOUW

PHYSICAL DYNAMICS INC.
P. O. BOX 10367
OAKLAND, CA. 94610
ATTN: A. THOMSON

R & D ASSOCIATES
P. O. BOX 9695
MARINA DEL REY, CA 90291
01CY ATTN FORREST GILMORE
01CY ATTN BRYAN GABBARD
01CY ATTN WILLIAM B. WRIGHT JR
01CY ATTN ROBERT F. LELEVIER
01CY ATTN WILLIAM J. KARZAS
01CY ATTN H. ORY
01CY ATTN C. MACDONALD
01CY ATTN R. TURCO

RAND CORPORATION, THE
1700 MAIN STREET
SANTA MONICA, CA 90406
01CY ATTN CULLEN CRAIN
01CY ATTN ED BEDROZIAN

RIVERSIDE RESEARCH INSTITUTE
80 WEST END AVENUE
NEW YORK, NY 10023
01CY ATTN VINCE TRAPANI

SCIENCE APPLICATIONS, INC.
P. O BOX 2351
LA JOLLA, CA 92038
01CY ATTN LEWIS M. LINSON
01CY ATTN DANIEL A. HAMLIN
01CY ATTN D. SACHS
01CY ATTN E. A. STRAKER
01CY ATTN CURTIS A. SMITH
01CY ATTN JACK MCDOUGALL

RAYTHEON CO.
528 BOSTON POST ROAD
SUDBURY, MA 01776
01CY ATTN BARBARA ADAMS

SCIENCE APPLICATIONS, INC.
1710 GOODRIDGE DR.
MCLEAN, VA 22102
ATTN: J. COCKAYNE

LOCKHEED MISSILE & SPACE CO., INC.
HUNTSVILLE RESEARCH & ENGR. CTR.
4800 BRADFORD DRIVE
HUNTSVILLE, ALABAMA 35807
ATTN: DALE H. DAVIS

MCDONNELL DOUGLAS CORPORATION
5301 BOLSA AVENUE
HUNTINGTON BEACH, CA 92647
01CY ATTN N. HARRIS
01CY ATTN J. MOULE
01CY ATTN GEORGE MROZ
01CY ATTN W. OLSON
01CY ATTN R. W. HALPRIN
01CY ATTN TECHNICAL LIBRARY SERVICES

MISSION RESEARCH CORPORATION
735 STATE STREET
SANTA BARBARA, CA 93101
01CY ATTN P. FISCHER
01CY ATTN W. F. CREVIER
01CY ATTN STEVEN L. GUTSCHE
01CY ATTN D. SAPPENFIELD
01CY ATTN R. BOGUSCH
01CY ATTN R. HENDRICK
01CY ATTN RALPH KILB
01CY ATTN DAVE SOWLE
01CY ATTN F. FAJEN
01CY ATTN M. SCHEIBE
01CY ATTN CONRAD L. LONGMIRE
01CY ATTN WARREN A. SCHLUETER

MITRE CORPORATION, THE
P. O. BOX 208
BEDFORD, MA 01730
01CY ATTN JOHN MORGANSTERN
01CY ATTN G. HARDING
01CY ATTN C. E. CALLAHAN

MITRE CORP
WESTGATE RESEARCH PARK
1820 DOLLY MADISON BLVD
MCLEAN, VA 22101
01CY ATTN W. HALL
01CY ATTN W. FOSTER

PACIFIC-SIERRA RESEARCH CORP
1456 CLOVERFIELD BLVD.
SANTA MONICA, CA 90404
01CY ATTN E. C. FIELD JR

PENNSYLVANIA STATE UNIVERSITY
IONOSPHERE RESEARCH LAB
318 ELECTRICAL ENGINEERING EAST
UNIVERSITY PARK, PA 16802
(NO CLASSIFIED TO THIS ADDRESS)
01CY ATTN IONOSPHERIC RESEARCH LAB

PHOTOMETRICS, INC.
442 MARRETT ROAD
LEXINGTON, MA 02173
01CY ATTN IRVING L. KOFSKY

TECHNOLOGY INTERNATIONAL CORP
75 WIGGINS AVENUE
BEDFORD, MA 01730
01CY ATTN W. P. BOQUIST

TRW DEFENSE & SPACE SYS GROUP
ONE SPACE PARK
REDONDO BEACH, CA 90278
01CY ATTN R. K. PLEBUCH
01CY ATTN S. ALTSCHULER
01CY ATTN D. DEE

Visidyne
5 Corporate Place
South Bedford St.
Burlington, Mass 01803

SRI INTERNATIONAL
333 RAVENSWOOD AVENUE
MENLO PARK, CA 94025
01CY ATTN DONALD NEILSON
01CY ATTN ALAN BURNS
01CY ATTN G. SMITH
01CY ATTN L. L. COBB
01CY ATTN DAVID A. JOHNSON
01CY ATTN WALTER G. CHESNUT
01CY ATTN CHARLES L. RINO
01CY ATTN WALTER JAYE
01CY ATTN M. BARON
01CY ATTN RAY L. LEADABRAND
01CY ATTN G. CARPENTER
01CY ATTN G. PRICE
01CY ATTN J. PETERSON
01CY ATTN R. HAKE, JR.
01CY ATTN V. GONZALES
01CY ATTN D. MCDANIEL

IONOSPHERIC MODELING DISTRIBUTION LIST
UNCLASSIFIED ONLY

Please distribute one copy to each of the following people:

Naval Research Laboratory
Washington, D.C. 20375

Dr. P. Mange - Code 4101
Dr. R. Meier - Code 4141
Dr. E. Szuszczewicz - Code 4187
Dr. J. Goodman - Code 4180

Science Applications, Inc.
1250 Prospect Plaza
La Jolla, California 92037

Dr. D. A. Hamlin
Dr. L. Linson
Dr. D. Sachs

Director of Space and Environmental
Laboratory, NOAA
Boulder, Colorado 80302

Dr. A. Glenn Jean
Dr. G. W. Adams
Dr. D. N. Anderson
Dr. K. Davies
Dr. R. F. Donnelly

A. F. Geophysics Laboratory
L. G. Hanscom Field
Bedford, Mass. 01730

Dr. T. Elkins
Dr. W. Swider
Mrs. R. Sagalyn
Dr. J. M. Forbes
Dr. T. J. Keneshea
Dr. J. Aarons

Dr. R. Narcisi
Office of Naval Research
800 North Quincy Street
Arlington, Virginia 22217

Dr. H. Mullaney

Commander
Naval Electronics Laboratory Center
San Diego, California 92152

Mr. R. Rose - Code 5321

U.S. Army Aberdeen Research and
Development Center
Ballistic Research Laboratory
Aberdeen, MD

Dr. J. Heimerl

Commander
Naval Air Systems Command
Department of the Navy
Washington, D.C. 20360

Dr. T. Czuba

Harvard University
Harvard Square
Cambridge, Mass. 02138

Dr. M. B. McElroy
Dr. R. Lindzen

Pennsylvania State University
University Park, Pennsylvania 16802

Dr. J. S. Nisbet
Dr. P. R. Rohrbaugh
Dr. L. A. Carpenter
Dr. M. Lee
Dr. R. Divany
Dr. P. Bennett
Dr. E. Klevans

University of California, Los Angeles
405 Hilgard Avenue
Los Angeles, California 90024

Dr. F. V. Coroniti
Dr. C. Kennel

University of California, Berkeley
Berkeley, California 94720

Dr. M. Hudson

Utah State University
4th N. and 8th Streets
Logan, Utah 84322

Dr. P. M. Banks
Dr. R. Harris
Dr. K. Baker

Cornell University
Ithaca, New York 14850

Dr. W. E. Swartz
Dr. R. Sudan
Dr. D. Farley
Dr. M. Kelley

NASA
Goddard Space Flight Center
Greenbelt, Maryland 20771

Dr. S. Chandra
Dr. K. Maeda
Dr. R.F. Benson

Princeton University
Plasma Physics Laboratory
Princeton, New Jersey 08540

Dr. F. Perkins
Dr. E. Frieman

Institute for Defense Analysis
400 Army/Navy Drive
Arlington, Virginia 22202

Dr. E. Bauer

University of Maryland
College Park, MD 20742

Dr. K. Papadopoulos
Dr. E. Ott

University of Pittsburgh
Pittsburgh, Pa. 15261

Dr. N. Zabusky
Dr. M. Biondi

Defense Documentation Center
Cameron Station
Alexandria, VA 22314

(12 copies if open publication
otherwise 2 copies)

12CY Attn TC

University of California
Los Alamos Scientific Laboratory
J-10, MS466
Los Alamos, New Mexico 87545

M. Pongratz
D. Simons

L. Duncan

S. Peter Gary
Massachusetts Institute of Technology
Plasma Fusion Center
Library, NW16-262
Cambridge, MA 02139


DATE
ILME